Communication

Enhanced Capacitive Humidity Sensing Performance at Room Temperature via Hydrogen Bonding of Cyanopyridone-Based Oligothiophene Donor

Salman Ali [1], Mohammed A. Jameel [1], Christopher J. Harrison [1], Akhil Gupta [1,2,*], Richard A. Evans [2], Mahnaz Shafiei [1,*] and Steven J. Langford [1,*]

[1] School of Science, Computing and Engineering Technologies, Swinburne University of Technology, Hawthorn, VIC 3122, Australia; salmanali@swin.edu.au (S.A.); mjameel@swin.edu.au (M.A.J.); cjharrisson@swin.edu.au (C.J.H.)

[2] CSIRO Manufacturing, Clayton South, VIC 3169, Australia; richard.evans@csiro.au

* Correspondence: akhilgupta@swin.edu.au (A.G.); mshafiei@swin.edu.au (M.S.); sjlangford@swin.edu.au (S.J.L.)

Abstract: Cyanopyridone-based oligothiophene donors with both hydrophobic and hydrophilic characters have been evaluated as active layers within simple capacitive devices for humidity sensing at room temperature. Surface studies using atomic force microscopy revealed a self-assembled nanofibrous network with a thin needle-like structure for the terminal hydroxy example (**CP6**), devoid in the methyl example (**CP1**). The sensing performance of each sensor was investigated over a broad range of relative humidity levels as a function of capacitance at room temperature. The sensor **CP6** demonstrated favourable features such as high sensitivity (12.2 pF/%RH), quick response/recovery (13 s/20.7 s), wide working range of relative humidity (10%–95% RH), low hysteresis (0.57%), outstanding recyclability, and excellent long-term stability. From the results obtained, hydrophilicity and hydrogen bonding appear to play a vital role in enhancing humidity sensing performance, leading to possible new design directions for simple organic semiconductor-based sensors.

Keywords: capacitive sensors; donor-acceptor; humidity; hydrogen bonding; self-assembly

1. Introduction

Humidity sensors are broadly applied in diverse disciplines, such as environmental monitoring [1,2], material preparation [3], agriculture [4], food processing [5], pharmaceutical preparation [6], wearable and flexible equipment [7], health services [8], high energy physics applications [9], as well as heating, ventilation, and air-conditioning [10]. Precision devices for humidity monitoring and measurement are essential in advanced scientific applications to meet high expectations for sensitivity, exceptional stability, and chemical compatibility. To date, a variety of materials, such as oxides, ceramics, composites, graphene, biomaterials, polymers, and small organic molecules [11–13] have been utilised in the development of capacitive, resistive, optical fibre, and quartz crystal microbalance types of humidity sensors [14]. Almost 75% of the commercially available humidity sensors are based on the capacitive technique. Capacitive humidity sensors present various benefits, comprising very low power consumption, good stability, and high output signals. In comparison with resistive type humidity sensors, capacitive ones have been described to demonstrate comparatively better stability, particularly considering the heavy condensation of water molecules amid high humidity levels [12].

Although several humidity sensor technologies have demonstrated considerable benefits, such as high sensitivity and convenient use, issues such as operation at room temperature, long-term stability, quick response and recovery, and limited detection range

are challenges that need attention [12]. Different types of materials and fabrication techniques have been used to overcome these challenges [12,15–17]. However, additional investigations are still necessary to improve sensing performance and broaden the range of acceptable materials for use. In this context, the development and utilisation of new organic materials with designer properties are crucial for improving the sensing performance and applicability of humidity sensors across a broad range of applications [18,19]. While polymers can provide a suitable one-pot process to organic active materials, the development of small-molecule systems through appropriate, rational design strategies, can offer considerably more, if realised.

Currently, small organic molecules, including the phthalocyanines (Pcs), perylene diimides (PDIs), naphthalene diimides (NDIs), and donor-conjugation–acceptor (D-π-A) materials, have demonstrated applicability in various electronic devices, such as sensors [12,18,20,21]. Small organic molecules can offer various advantages, including straightforward synthetic protocols, defined molecular weight, simple purification and structural modification, good batch-to-batch reproducibility, and excellent solution-processability [22] over the other types of materials. Furthermore, their structural, electronic, and surface properties can be easily tuned via molecular engineering using the correct pre-programming of components [23–25].

In the current work, we investigate the capacitive humidity sensing performance of molecularly engineered oligothiophene donor **CP6** (Figure 1a), which is a composite and elongated D-π-A molecular system bearing triphenylamine and cyanopyridone functionalities as donor and acceptor, respectively, within a π-conjugated organic semiconducting material. While designing **CP6**, we opted to utilise N-substitution of the cyanopyridone functionality to stimulate self-assembly through hydrogen bonding. The justification behind this concept lies in the fact that N-substitution of cyanopyridone lies out of the molecular plane and does not affect molecular electronics. Additionally, any alteration on N-substitution will not substantially change the aligning of the HOMO and the LUMO energy levels, and any variations in thin film properties, e.g., morphology, can be primarily linked to the capability of the compound to self-assemble, and as a result it can enhance the sensing performance. **CP6** carries a vital structural component, a terminal hydroxyethoxy group (as an H-bond acceptor), which is not only useful for enhanced interaction with water molecules, but also to promote intramolecular interactions between molecules in the layer through hydrogen bonding, that could lead to marked changes in capacitive performance in humidity sensing [18,19]. In this case, we hope to improve capacitive type humidity sensing using those motifs, which can promote assembly into nanofibrous networks upon evaporation from common aprotic non-polar processing solvents, such as chloroform and xylene. A control sensing experiment, where a simple alkyl-substituted cyanopyridone-based oligothiophene donor, **CP1**, was applied to authenticate the effect of the hydroxyethoxy group on humidity sensing performance, is shown in Figure 1b. Through this comparison, we hope to show that the variation of substituent groups at the cyanopyridone-based oligothiophene donors' imide position can markedly affect the surface morphology and thus, significantly improve sensing performance.
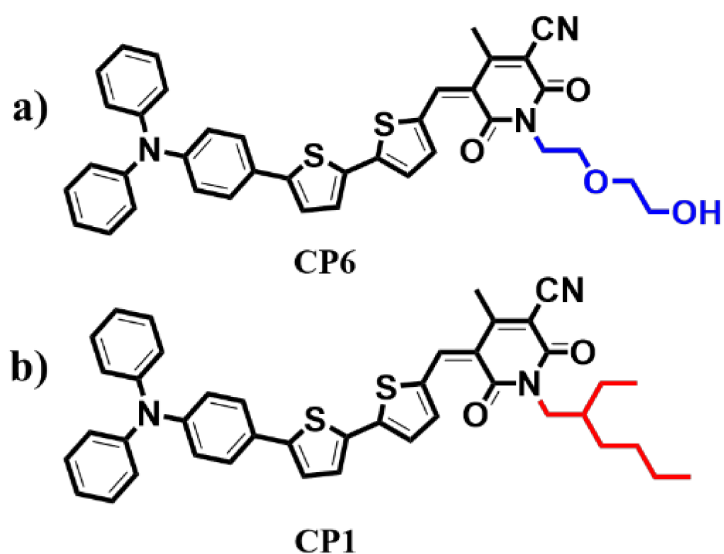
Figure 1. Chemical structures of (**a**) **CP6** and (**b**) **CP1**.

2. Materials and Methods

2.1. Synthesis

The chemical synthesis of the materials used in this work, Figure 1, has been reported in our previous studies [26,27].

2.2. Device Fabrication and Characterisation

For the fabrication of sensors, interdigitated electrodes (IDEs) (10 × 6 × 0.75 mm dimensions with 10 μm gap between the fingers deposited over glass substrate) were purchased from Micrux technologies and cleaned prior to use by sonicating in isopropanol and acetone, followed by deionised water. The IDEs were dried by applying nitrogen gas and were kept in an oven at 80 °C overnight to dry out any remaining contaminations. Solutions of **CP6** and **CP1** in *o*-xylene (10 mg/mL) were prepared and spin-coated over clean IDEs and Si substrates at 2000 rpm for 1 min to produce thin films for sensor device and characterisations, respectively. Surface analyses of the prepared films were carried out using atomic force microscopy (AFM) run in a semi-tapping mode at a frequency of 0.89 Hz. Humidity sensing measurements of the prepared sensors were carried out at 24 ± 0.5 °C room temperature (RT) in a custom-built, fully automated multi-channel gas calibration system consisting of mass flow controllers (MFCs), a LINKAM HFS600E chamber and a LINKAM RH95 humidity generator, in which humidity is controlled through synthetic air. The humidity generator is supplied with dry air, which is then saturated by bubbling through water. The generator controls the proportion of flow from the dry source vs. the saturated source to achieve the desired level of humidity. Closed-loop regulation is used to maintain the desired humidity level. The capacitive humidity sensing response was recorded by GW-INSTEK LCR-6100 at 250 Hz and 1 V. Sensitivity to humidity was calculated using the following Equation (1):

$$S = \frac{C_{RH(max)} - C_{RH(min)}}{RH_{max} - RH_{min}} \qquad (1)$$

where S is the sensitivity, $C_{RH(max)}$ is the capacitance at a maximum relative humidity in the active region, $C_{RH(min)}$ is the capacitance at a minimum relative humidity in the active region, and RH_{max} and RH_{min} are the maximum and minimum relative humidity levels in the active region, respectively.

3. Results and Discussions

3.1. Surface and Structural Analyses

The AFM analysis was carried out to observe the surface morphology of **CP6** thin film and the results are shown in Figure 2. It is evident that **CP6** assembled into a continuous nanofibrous network through the needle-like structures, which offered a high surface area for interaction with water molecules and, as a result, should improve sensing performance. **CP1**, on the other hand, afforded an amorphous surface, as reported in our earlier work [26].
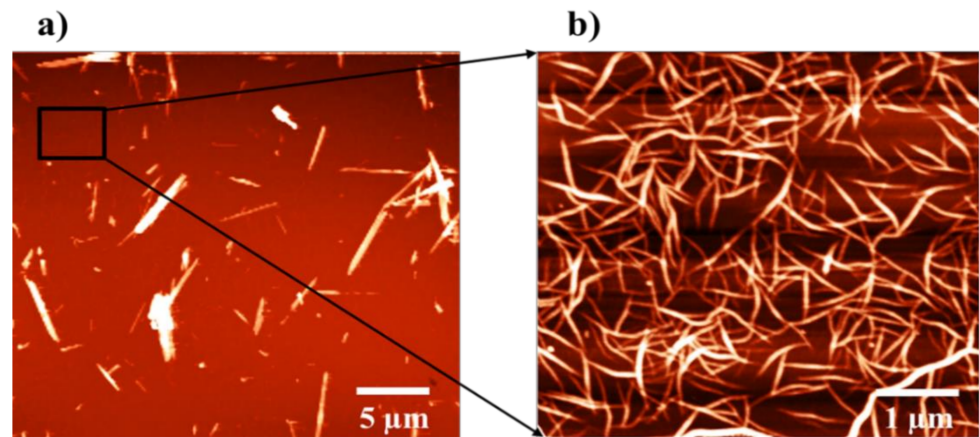

Figure 2. (**a**) AFM images of the **CP6** film at 5 μm; (**b**) at 1 μm.

3.2. Humidity Sensing Studies

Sensing performance within capacitive humidity sensors is affected by the applied frequency [28]. To clearly understand the effect, the capacitance of the **CP6**-based sensor was recorded at numerous functioning frequencies—100 Hz, 250 Hz, 500 Hz, 1 kHz, and 2 kHz—over the range of 0% to 95% relative humidity (RH) at RT, as shown in Figure 3. In addition, the log capacitance-relative humidity relation is specifically given to observe the change in capacitance at low RH levels clearly. The **CP6**-based sensor showed the highest sensitivity at 100 Hz. However, the application of frequency higher than 100 Hz for capacitive humidity sensors is commonly recommended to diminish any interface-trapped charge carriers, creating excess capacitance through polarisation [29]. Therefore, 250 Hz was selected as a pragmatic operating frequency for humidity sensing experiments in order to accomplish better repeatability and stability.
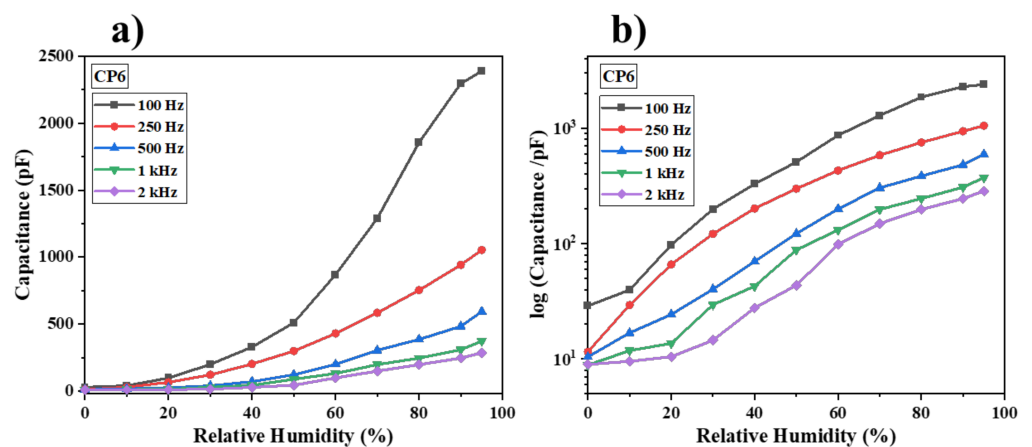

Figure 3. (**a**) Capacitance-humidity and (**b**) log capacitance-humidity relationship of the **CP6**-based sensor at different frequencies.

The capacitance curve of the **CP6** based sensor as a function of RH increase is shown in Figure 4a, and compared with **CP1**. The capacitance of the prototype humidity sensor

bearing **CP6** increased approximately 90 times by magnitude as the relative humidity was increased from 0% to 95% RH, which is significantly higher when compared with **CP1**, devoid of any hydrophilic characters. At lower humidity levels, i.e., from 0% to 30% RH, there is a modest increase in capacitance due to a smaller number of adsorbed water vapours, which are not enough to substantially increase in the dielectric constant of the sensing layer. However, even within that range, there is a marked difference in capacitance between **CP6** and **CP1**. Above 30% RH, there appears to be a substantial increase in the capacitance, corresponding to the increase in the relative permittivity of the material as a result of the higher content of moisture adsorption over the film surface. The **CP6**-based sensor shows excellent sensitivity (12.2 pF/%RH), which is higher than the sensitivity reported in the literature using other D-π-A type materials (i.e., 0.064 and 0.012 pF/%RH, respectively [30,31]). **CP1** demonstrated comparably lower sensitivity (0.43 pF/%RH) as shown in Figure 4a. These findings validate the fact that the presence of the hydrophilic hydroxyethoxy group on **CP6** indeed plays a significant role in the signalling process.
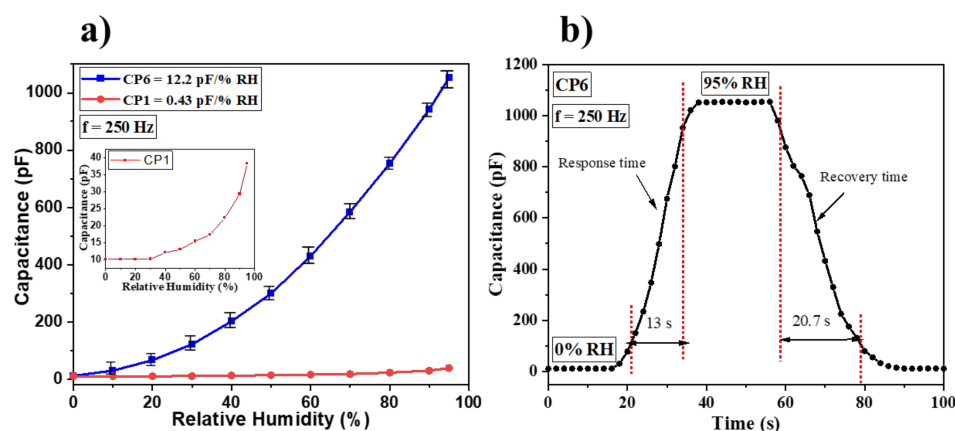

Figure 4. (**a**) Capacitance of **CP6**- and **CP1**-based sensors as a function of RH. Inset: Capacitance of **CP1** as a function of RH and (**b**) response and recovery curves for **CP6** sensor at 250 Hz.

Figure 4b demonstrates the response and recovery profile of the sensor with a **CP6** active layer to 95% RH. The capacitance of the sensor increases quickly when the sensor is exposed to 95% RH and importantly, falls to the initial value when the sensor is then exposed to 0% RH. The response or recovery time is defined as the time needed for the sensor to vary its capacitance from 10% to 90% of its final value [32]. The **CP6**-based sensor displays a quick response (13 s) and recovery (20.7 s). Table 1 compares these values with the recently reported systems using inorganic, hybrid, polymer, and small organic active layers, indicating their overall high performance and validates our approach.

The humidity sensing mechanism can be described by two successive processes: Chemisorption and physisorption [33]. At low RH, water molecules are primarily physisorbed onto the existing active sites of the **CP6** surface through double hydrogen bonding, as shown in Figure 5. In this regime, the water molecules cannot move freely due to the double hydrogen bonding constraints. The hopping transfer of protons between adjacent hydroxyl groups in the first-layer physical adsorption of water molecules requires a large amount of energy. As the RH increases, water molecules are physisorbed via single hydrogen bonding on the hydroxyl groups. Subsequently, the water molecules aquire higher mobility and gradually become similar to those in the bulk liquid. In the bulk liquid, proton hopping between the neighbouring water molecules happens in the sensing film, with the charge transport generated by a Grotthuss chain reaction ($H_2O + H_3O^+ = H_3O^+ + H_2O$) [34]. In this situation, the electric field ionises the water molecules, which produce hydronium ions (H_3O^+) as charge carriers, which produce protons ($H_3O^+ \rightarrow H_2O + H^+$) due to hydration. These protons need very low energy for hopping between the adjacent water molecules. As a result, the ionic conductivity increases [35]. Conduction at a relatively low level of %RH is mainly centered on H^+

jumping due to the low adsorption rate of water vapours. Increasing the %RH level in the humidity chamber of the sensor results in the formation of more H^+ ions and the creation of hydrogen bonds between the sensing material and water vapours, which speed up their flow in the functional layer. A schematic diagram of the potential humidity sensing mechanism is shown in Figure 5.
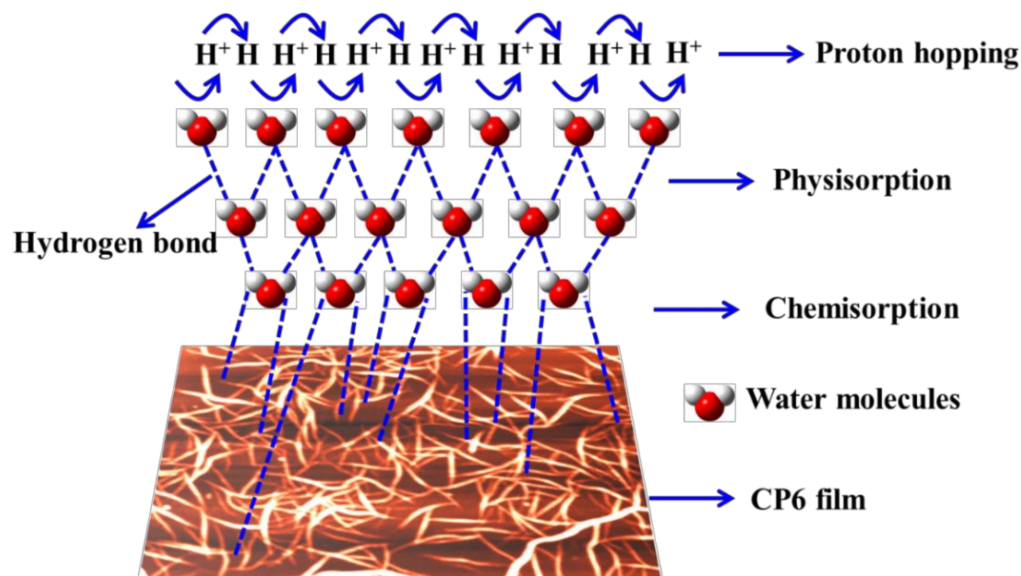

Figure 5. Proposed humidity sensing mechanism.

Hysteresis describes the lead or lag of capacitance in the desiccation of the humidity sensor with respect to the humidification process, defined as the percentage of maximum capacitance difference below a particular humidity level to the capacitance difference in the whole recorded humidity range [36]. As illustrated in Figure 6a, during the process of the ascending RH from 0% to 95% and then descending to 0%, the two recorded curves of adsorption and desorption as a measure of capacitance are very close. The hysteresis (H) can be determined using Equation [37]:

$$H = \Delta H_{max} / 2S \tag{2}$$

where ΔH_{max} is the divergence between the response of humidity sensor towards the same RH value through adsorption and desorption operations, and S is the sensitivity. The maximum hysteresis is only 0.53% at 50% RH, implying that the sensor has a small hysteresis, substantially less than reported in previous works (Table 1). The hysteresis curve is zigzag since the rate of water vapour adsorption and deportation is not the same over the surface of the sensing layer. Furthermore, to check the sensor's recyclability, the sensor was exposed to 0% and 95% RH over four cycles. The sensor displayed excellent recyclability as shown in Figure 6b. To investigate the long-term stability of the **CP6**-based sensor, the capacitance was recorded at different RH levels (0% to 95%) for 4 weeks, and the result is shown in Figure 6c. The sensor displayed outstanding accuracy in the capacitance value after every week with a minimum deviation. The sensitivity of the **CP6**-based sensor decreased from 12.2 to 11.9 pF/%RH after 4 weeks.
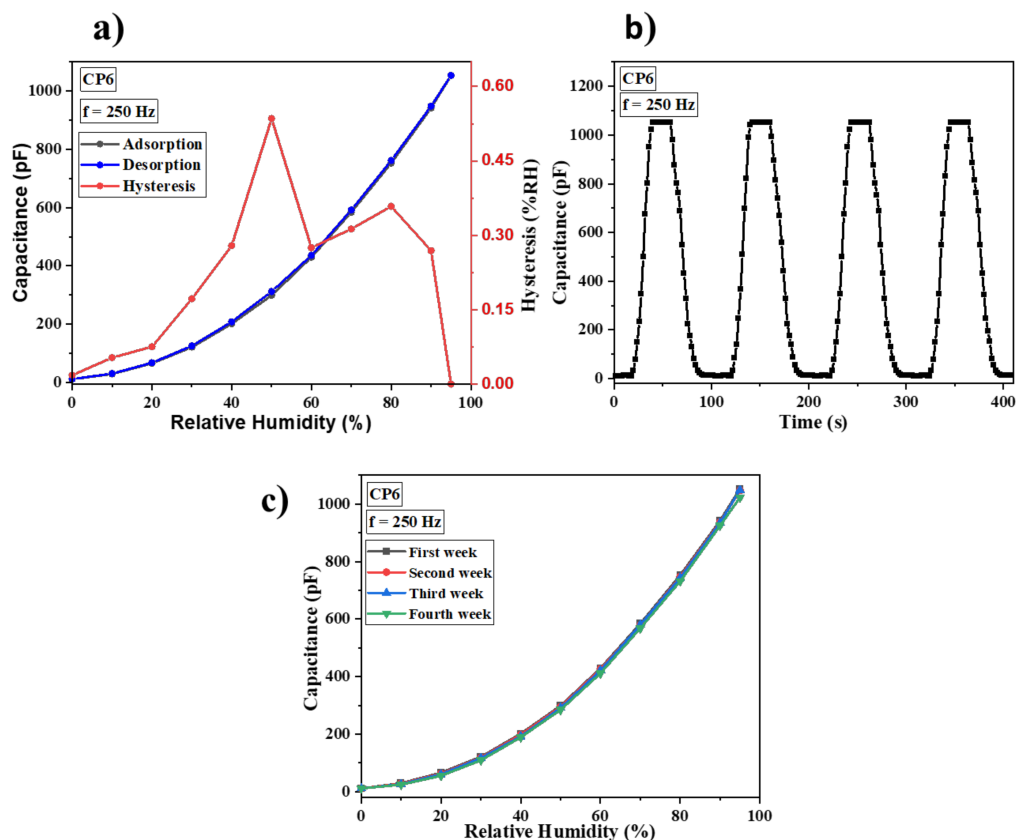
Figure 6. (**a**) Hysteresis, (**b**) recyclability, and (**c**) stability curves of the **CP6**-based sensor from 0% to 95% RH at 250 Hz.

Table 1. A comparative study of the **CP6**-based sensor with recently reported humidity sensors.

Materials	Bandwidth (%RH)	Operating Frequency	Hysteresis (%)	T_{Res}/T_{Rec} (s)	Sensitivity (pF/%RH)	Refs.
PANI/Cu–ZnS	30–90	-	1.5	42/24	12	[33]
AU/PVA	11–93	-	-	145/94	0.05	[38]
NDI-1	10–95	250 Hz	0.72	20.1/6.28	10.13	[39]
ZnPc	20–100	1 kHz	9.13	15/10	1.03	[40]
$CoCr_2O_4$	05–95	100 Hz	-	100/150	3	[41]
VTP	30–95	500 Hz	1.26	15/10	0.09	[42]
AAQ	40–88	120 Hz	-	20/26	0.4	[43]
$PBObzT_2$	50–95	100 Hz	2.76	10/4	5	[44]
TMBHPET	37–99	100 Hz	2.4	15/15	0.064	[30]
DMBHPET	45–95	1 kHz	-	10/15	0.012	[31]
PDI derivative	60–90	120 Hz	-	60/70	41	[45]
NDI derivative	10–95	250 Hz	2.06	374/607	475	[18]
Porous polymer	15–80	-	9.08	-	0.4	[46]
GrF	15–86	100 Hz	-	0.4/4	7.77	[47]
P(VDF-TrFE)	08–98	100 Hz	-	0.8/2.5	0.05	[48]
MOF NPs	04–88	-	-	420/510	0.35	[49]
CP6	10–95	250 Hz	0.53	13/20.7	12.2	This work

Schematic diagram of equivalent circuit of the **CP6** sensor is shown in Figure 7, where *Ca* represents the capacitance due to the dielectric of air-filled in the film. The *Ceff* denotes the capacitance due to the dielectric of **CP6** affected by the relative humidity, the capacitance, *Cg*, is due to the dielectric of the substrate, and the dielectric of air and substrate is negligible compared with the dielectric of the sensing material **CP6** when exposed to relative humidity.
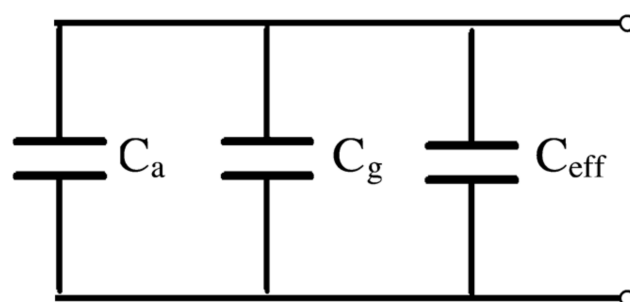
Figure 7. Schematic diagram of an electrical equivalent circuit model of the **CP6**-based sensor.

4. Conclusions

A high-performance capacitive type humidity sensor based on an elongated D-π-A bearing triphenylamine–oligothiophene-cyanopyridone motif (as **CP6**) was successfully developed, and its sensing properties were investigated in detail. The sensing parameters, such as, sensitivity, response/recovery times, hysteresis, and long-term stability, were studied, revealing the excellent sensing performance. The **CP6**-based sensor showed higher sensitivity when compared with the sensor based on its structural analogue **CP1**, which can be attributed to the presence of the hydrophilic hydroxyethoxy group on the cyanopyridone fragment of **CP6**. The hydroxyethoxy group played an essential role in generating hydrogen bonding between the adsorbed water molecules and the **CP6** film surface. It is noteworthy to mention that the humidity sensing performance of the **CP6**-based capacitive device exhibits favourable properties to frequently used materials, but also provides a strong economical platform for lab-to-fab transition. We believe that the presented results and discussed analysis provide considerable theoretical and technological advances to develop high-performing humidity sensors based on D-π-A oligothiophenes. Considering the high sensing performance of our prototype sensor, we believe that it has the potential to sense the moisture content in the human breath, as well as non-contact skin humidity sensing. Breath analysis is seen as an essential method to examine the physiological state of the human body that retains numerous benefits, including non-invasiveness, well-being, and user-friendliness, while non-contact humidity sensing has applications where common sweaty exteriors, such as palmar hyperhidrosis, could be diagnosed. Therefore, in our upcoming work, we will focus on the above-mentioned application of these types of sensors.

Conflicts of Interest: The authors declare no conflict of interest.

References

1. Peng, Y.; Zhao, Y.; Chen, M.-Q.; Xia, F. Research advances in microfiber humidity sensors. *Small* **2018**, *14*, e1800524. [CrossRef]
2. Huang, T.; Chou, J.; Sun, T.; Hsiung, S. A device for skin moisture and environment humidity detection. *Sens. Actuators B Chem.* **2008**, *134*, 206–212. [CrossRef]
3. Kuwahara, Y.; Tamagawa, S.; Fujitani, T.; Yamashita, H. Removal of phosphate from aqueous solution using layered double hydroxide prepared from waste iron-making slag. *Bull. Chem. Soc. Jpn.* **2016**, *89*, 472–480. [CrossRef]
4. Antonacci, A.; Arduini, F.; Moscone, D.; Palleschi, G.; Scognamiglio, V. Nanostructured (Bio)sensors for smart agriculture. *TrAC Trends Anal. Chem.* **2018**, *98*, 95–103. [CrossRef]
5. Lang, C.; Hubert, T.; Quaas, H.; Linke, M. Online measurement of humidity in the agri-food chain. *Acta Hortic.* **2010**, 413–417. [CrossRef]
6. Bridgeman, D.; Corral, J.; Quach, A.; Xian, X.; Forzani, E. Colorimetric humidity sensor based on liquid composite materials for the monitoring of food and pharmaceuticals. *Langmuir* **2014**, *30*, 10785–10791. [CrossRef] [PubMed]
7. Lan, L.; Le, X.; Dong, H.; Xie, J.; Ying, Y.; Ping, J. One-step and large-scale fabrication of flexible and wearable humidity sensor based on laser-induced graphene for real-time tracking of plant transpiration at bio-interface. *Biosens. Bioelectron.* **2020**, *165*, 112360. [CrossRef]
8. Salimifard, P.; Rim, D.; Gomes, C.; Kremer, P.; Freihaut, J.D. Resuspension of biological particles from indoor surfaces: Effects of humidity and air swirl. *Sci. Total Environ.* **2017**, *583*, 241–247. [CrossRef] [PubMed]
9. Berruti, G.; Consales, M.; Giordano, M.; Sansone, L.; Petagna, P.; Buontempo, S.; Breglio, G.; Cusano, A. Radiation hard humidity sensors for high energy physics applications using polyimide-coated fiber Bragg gratings sensors. *Sens. Actuators B Chem.* **2013**, *177*, 94–102. [CrossRef]
10. Png, E.; Srinivasan, S.; Bekiroglu, K.; Chaoyang, J.; Su, R.; Poolla, K. An internet of things upgrade for smart and scalable heating, ventilation and air-conditioning control in commercial buildings. *Appl. Energy* **2019**, *239*, 408–424. [CrossRef]
11. Kaushik, A.; Kumar, R.; Arya, S.K.; Nair, M.; Malhotra, B.D.; Bhansali, S. Organic-inorganic hybrid nanocomposite-based gas sensors for environmental monitoring. *Chem. Rev.* **2015**, *115*, 4571–4606. [CrossRef]
12. Najeeb, M.A.; Ahmad, Z.; Shakoor, R.A. Organic thin-film capacitive and resistive humidity sensors: A focus review. *adv. mater. interfaces* **2018**, *5*, 1800969. [CrossRef]
13. Rehman, H.M.U.; Rehman, M.; Saqib, M.; Khan, S.A.; Khan, M.; Yang, Y.; Kim, S.; Rahman, S.; Kim, W.-Y. Highly efficient and wide range humidity response of biocompatible egg white thin film. *Nanomaterials* **2021**, *11*, 1815. [CrossRef] [PubMed]
14. Rittersma, Z. Recent achievements in miniaturised humidity sensors—A review of transduction techniques. *Sens. Actuators A Phys.* **2002**, *96*, 196–210. [CrossRef]
15. Ali, S.; Hassan, A.; Hassan, G.; Bae, J.; Lee, C.H. All-printed humidity sensor based on graphene/methyl-red composite with high sensitivity. *Carbon* **2016**, *105*, 23–32. [CrossRef]
16. Farahani, H.; Wagiran, R.; Hamidon, M.N. Humidity sensors principle, mechanism, and fabrication technologies: A comprehensive review. *Sensors* **2014**, *14*, 7881–7939. [CrossRef]
17. Fatima, N.; Aziz, F.; Ahmad, Z.; Najeeb, M.A.; Azmeer, M.I.; Karimov, K.S.; Ahmed, M.M.; Basheer, S.; Shakoor, R.A.; Sulaiman, K. Compositional engineering of the pi-conjugated small molecular VOPcPhO: Alq3 complex to boost humidity sensing. *RSC Adv.* **2017**, *7*, 19780–19786. [CrossRef]
18. Ali, S.; Jameel, M.A.; Gupta, A.; Langford, S.J.; Shafiei, M. Capacitive humidity sensing performance of naphthalene diimide derivatives at ambient temperature. *Synth. Met.* **2021**, *275*, 116739. [CrossRef]
19. Fatima, Q.; Haidry, A.A.; Yao, Z.; He, Y.; Li, Z.; Sun, L.; Xie, L. The critical role of hydroxyl groups in water vapor sensing of graphene oxide. *Nanoscale Adv.* **2019**, *1*, 1319–1330. [CrossRef]
20. Ali, S.; Gupta, A.; Shafiei, M.; Langford, S. Recent advances in perylene diimide-based active materials in electrical mode gas sensing. *Chemosensors* **2021**, *9*, 30. [CrossRef]
21. Wahab, F.; Sayyad, M.H.; Khan, D.N.; Tahir, M.; Aziz, F.; Khan, R.; Karimov, K.S. Sensing properties of cobalt-phthalocyanine-based multipurpose sensor. *J. Electron. Mater.* **2017**, *46*, 2045–2052. [CrossRef]
22. Bronstein, H.; Nielsen, C.B.; Schroeder, B.C.; McCulloch, I. The role of chemical design in the performance of organic semiconductors. *Nat. Rev. Chem.* **2020**, *4*, 66–77. [CrossRef]
23. Bhosale, S.V.; Jani, C.H.; Langford, S.J. Chemistry of naphthalene diimides. *Chem. Soc. Rev.* **2008**, *37*, 331–342. [CrossRef]
24. Chen, S.; Slattum, P.; Wang, C.; Zang, L. Self-assembly of perylene imide molecules into 1d nanostructures: Methods, morphologies, and applications. *Chem. Rev.* **2015**, *115*, 11967–11998. [CrossRef]
25. Hundal, A.K.; Agarwal, A.; Jameel, M.A.; Ali, S.; Chen, J.-Y.; Kaur, N.; Jones, L.; Li, J.-L.; Langford, S.; Gupta, A. Impact of self-assembly on the photovoltaic properties of a small molecule oligothiophene donor. *Sol. Energy* **2020**, *195*, 223–229. [CrossRef]
26. Hundal, A.K.; Ali, S.; Agarwal, A.; Jameel, M.A.; Jones, L.A.; Li, J.-L.; Evans, R.A.; Langford, S.J.; Gupta, A. Enhanced photovoltaic efficiency via control of self-assembly in cyanopyridone-based oligothiophene donors. *J. Phys. Chem. Lett.* **2021**, *12*, 919–924. [CrossRef]

27. Gupta, A.; Ali, A.; Bilic, A.; Gao, M.; Hegedűs, K.; Singh, B.; Watkins, S.E.; Wilson, G.J.; Bach, U.; Evans, R.A. Absorption enhancement of oligothiophene dyes through the use of a cyanopyridone acceptor group in solution-processed organic solar cells. *Chem. Commun.* **2012**, *48*, 1889–1891. [CrossRef] [PubMed]

28. Tripathy, A.; Pramanik, S.; Manna, A.; Bhuyan, S.; Shah, N.F.A.; Radzi, Z.; Abu Osman, N.A. Design and development for capacitive humidity sensor applications of lead-free Ca,Mg,Fe,Ti-oxides-based electro-ceramics with improved sensing properties via physisorption. *Sensors* **2016**, *16*, 1135. [CrossRef]

29. Zhang, Y.; Wu, J.; Zhang, Y.; Guo, W.; Ruan, S. Characterization and humidity sensing properties of the sensor based on Na2Ti3O7 nanotubes. *J. Nanosci. Nanotechnol.* **2014**, *14*, 4303–4307. [CrossRef] [PubMed]

30. Al-Sehemi, A.G.; Al-Assiri, M.S.; Kalam, A.; Zafar, Q.; Azmer, M.I.; Sulaiman, K.; Ahmad, Z. Sensing performance optimization by tuning surface morphology of organic (D-π-A) dye-based humidity sensor. *Sens. Actuators B Chem.* **2016**, *231*, 30–37. [CrossRef]

31. Azmer, M.I.; Ahmad, Z.; Sulaiman, K.; Al-Sehemi, A.G. Humidity dependent electrical properties of an organic material DMBHPET. *Measurement* **2015**, *61*, 180–184. [CrossRef]

32. Li, B.; Tian, Q.; Su, H.; Wang, X.; Wang, T.; Zhang, D. High sensitivity portable capacitive humidity sensor based on In2O3 nanocubes-decorated GO nanosheets and its wearable application in respiration detection. *Sens. Actuators B Chem.* **2019**, *299*, 126973. [CrossRef]

33. Parangusan, H.; Bhadra, J.; Ahmad, Z.; Mallick, S.; Touati, F.; Al-Thani, N. Capacitive type humidity sensor based on PANI decorated Cu–ZnS porous microspheres. *Talanta* **2020**, *219*, 121361. [CrossRef] [PubMed]

34. Chen, Z.; Lu, C. Humidity sensors: A review of materials and mechanisms. *Sens. Lett.* **2005**, *3*, 274–295. [CrossRef]

35. Singh, H.; Tomer, V.K.; Jena, N.; Bala, I.; Sharma, N.; Nepak, D.; Pal, S.K. Truxene based porous, crystalline covalent organic frameworks and it's applications in humidity sensing. *Molecules* **2017**, *49*, 50.

36. Niu, H.; Yue, W.; Li, Y.; Yin, F.; Gao, S.; Zhang, C.; Kan, H.; Yao, Z.; Jiang, C.; Wang, C. Ultrafast-response/recovery capacitive humidity sensor based on arc-shaped hollow structure with nanocone arrays for human physiological signals monitoring. *Sens. Actuators B Chem.* **2021**, *334*, 129637. [CrossRef]

37. Khadse, V.; Thakur, S.; Patil, K.; Patil, P. Humidity-sensing studies of cerium oxide nanoparticles synthesized by non-isothermal precipitation. *Sens. Actuators B Chem.* **2014**, *203*, 229–238. [CrossRef]

38. Yao, W.; Chen, X.; Zhang, J. A capacitive humidity sensor based on gold–PVA core–shell nanocomposites. *Sens. Actuators B Chem.* **2010**, *145*, 327–333. [CrossRef]

39. Ali, S.; Jameel, M.A.; Harrison, C.J.; Gupta, A.; Shafiei, M.; Langford, S.J. Nanoporous naphthalene diimide surface enhances humidity and ammonia sensing at room temperature. *Sens. Actuators B Chem.* **2021**, *351*, 130972. [CrossRef]

40. Safian, N.A.M.; Anuar, A.; Omar, A.-Z.; Bawazeer, T.M.; Alsenany, N.; Alsoufi, M.S.; Supangat, A.; Roslan, N.A. Enhanced sensitivity of zinc phthalocyanine-based microporous humidity sensors by varying size of electrode gaps. *Sens. Actuators B Chem.* **2021**, *343*, 130158. [CrossRef]

41. Mondal, P.P.; Mahapatra, P.L.; Das, S.; Saha, D. Study on the novel capacitive moisture sensing behaviour of nickel chromite nanoparticle based thick film. *Measurement* **2020**, *163*, 107992. [CrossRef]

42. Roslan, N.A.; Abu Bakar, A.; Bawazeer, T.M.; Alsoufi, M.S.; Alsenany, N.; Majid, W.H.A.; Supangat, A. Enhancing the performance of vanadyl phthalocyanine-based humidity sensor by varying the thickness. *Sens. Actuators B Chem.* **2019**, *279*, 148–156. [CrossRef]

43. Ali, S.; Tahir, M.; Mehboob, N.; Wahab, F.; Langford, S.J.; Said, S.M.; Sarker, M.R.; Julai, S.; Ali, S.H.M. Amino anthraquinone: Synthesis, characterization, and its application as an active material in environmental sensors. *Material* **2020**, *13*, 960. [CrossRef]

44. Raza, E.; Asif, S.; Aziz, F.; Azmer, M.I.; Malik, H.A.; Teh, C.-H.; Najeeb, M.A.; Zafar, Q.; Ahmad, Z.; Wahab, F.; et al. Influence of thermal annealing on a capacitive humidity sensor based on newly synthesized macroporous PBObzT. *Sens. Actuators B Chem.* **2016**, *235*, 146–153. [CrossRef]

45. Tahir, M.; Sayyad, M.H.; Clark, J.; Wahab, F.; Aziz, F.; Shahid, M.; Chaudry, J.A. Humidity, light and temperature dependent characteristics of Au/N-BuHHPDI/Au surface type multifunctional sensor. *Sens. Actuators B* **2014**, *192*, 565–571. [CrossRef]

46. Tousi, M.M.; Zhang, Y.; Wan, S.; Yu, L.; Hou, C.; Yan, N.; Fink, Y.; Wang, A.; Jia, X. Scalable fabrication of highly flexible porous polymer-based capacitive humidity sensor using convergence fiber drawing. *Polymers* **2019**, *11*, 1985. [CrossRef]

47. Saqib, M.; Khan, S.A.; Mutee Ur Rehman, H.M.; Yang, Y.; Kim, S.; Rehman, M.M.; Young Kim, W. High-performance humidity sensor based on the graphene flower/zinc oxide composite. *Nanomaterials* **2021**, *11*, 242. [CrossRef]

48. Khan, S.A.; Saqib, M.; Rehman, M.M.; Mutee Ur Rehman, H.M.; Rahman, S.A.; Yang, Y.; Kim, W.Y. A full-range flexible and printed humidity sensor based on a solution-processed p (vdf-trfe)/graphene-flower composite. *Nanomaterials* **2021**, *11*, 1915. [CrossRef]

49. Andrés, M.A.; Vijjapu, M.T.; Surya, S.G.; Shekhah, O.; Salama, K.N.; Serre, C.; Eddaoudi, M.; Roubeau, O.; Gascón, I. Methanol and humidity capacitive sensors based on thin films of MOF nanoparticles. *ACS Appl. Mater. Interfaces* **2020**, *12*, 4155–4162. [CrossRef]